

A Proto-Galaxy Candidate at $z = 2.7$ Discovered by Its Young Stellar Population

H. K. C. Yee^{1,2,3}, E. Ellingson^{3,4}, Jill Bechtold⁵, R. G. Carlberg⁶, J.-C. Cuillandre^{3,7}

ABSTRACT

A protogalaxy candidate at $z = 2.72$ has been discovered serendipitously by the CNOC cluster redshift survey. The candidate is an extremely luminous ($V = 20.5$ mag, absolute mag -26) and well resolved ($2'' \times 3''$) disk-like galaxy. The redshift is identified from a dozen strong UV absorption lines, including lines with P-Cygni profiles, which are indicative of the presence of young O and B stars. No emission lines are found between 1000 and 2000Å (rest), including Ly α . The surface brightness profile of the galaxy fits an exponential law with a scale length of ~ 3.5 kpc. The multi-color photometric data fit the spectral energy distributions of a stellar population from 400 million years to an arbitrary young age, dependent on the amount of dust extinction. However, the presence of a strong P-Cygni profile in CIV $\lambda 1550$ indicates that a very substantial component of the stellar population must be younger than ~ 10 Myr. These models predict that this galaxy will evolve into a bright galaxy of several L^* in brightness. We can interpret this object as an early-type galaxy observed within about 100 million years of the initial burst of star formation which created most of its stellar mass, producing the extremely high luminosity. Because of the resolved, regular, and smooth nature of the object, it is unlikely that the high luminosity is due to gravitational lensing. We estimate the sky density of this type of objects observable at any one time to be $10^{0\pm 1}$ per square degree.

¹Department of Astronomy, University of Toronto, Toronto, Ontario M5S 1A7, Canada, Email: hyee@astro.utoronto.ca

²Canada-France-Hawaii Telescope, P.O.Box 1597, Kamuela, Hawaii 96743

³Guest observer, Canada-France-Hawaii Telescope, operated jointly by the NRC of Canada, CNRS of France, and the University of Hawaii

⁴CASA, University of Colorado, Campus Box 389, Boulder, CO 80309-0389, Email: e.elling@casa.colorado.edu

⁵Steward Observatory, University of Arizona, Tucson AZ 85721, Email: jbechtold@as.arizona.edu

⁶Department of Astronomy, University of Toronto, Toronto, Ontario M5S 1A7, Canada, Email: carlberg@astro.utoronto.ca

⁷Laboratoire d'Astrophysique de Toulouse Observatoire Midi-Pyrénées, UPS, 14 Av. E. Belin, 31400 Toulouse, France, Email: cuilland@srvdec.obs-mip.fr

1. Introduction

The discovery of a primeval, or proto-, galaxy – loosely defined as a galaxy in its initial star formation stage – has long been one of the most sought-after observational goals of extragalactic astronomy. The importance of proto-galaxies (PGs) to our understanding of the formation of structures and evolution of galaxies is enormous. By observing galaxies in their early stages of evolution, we may be able to delineate the dynamical processes that lead to and accompany the formation of galaxies. Furthermore, because evolution is slow for galaxies containing mostly stars older than about 1 Gyr (Tinsley 1972), it is only by observing the properties of galaxies during the first Gyr or so of their lifetime that we will be able to place strong constraints on the star formation and chemical evolution history of galaxies.

It is precisely because no definitive observational data for PG exist, that over the years PGs have been predicted to have properties covering the whole imaginable range of morphologies, colors, redshift of formation, and emission-line characteristics (e.g., see the excellent reviews by Koo 1986 and Pritchet 1994, and references therein). In response to the predictions arising from these diverse models of PGs, many different methods have been suggested and carried out in their search – narrow-band imaging from the near-UV to the infrared searching for Ly α emission (e.g., Pritchet & Hartwick 1990); broad-band imaging searches for the Lyman break (e.g., Steidel & Hamilton 1993, Djorgovski 1992); and searching around other known high-redshift objects discovered by their non-stellar emission, such as quasars, radio-galaxies, and damped Ly α absorbers (e.g., Djorgovski 1985, McCarthy 1993, and Wolfe 1995). Most of these searches have one thing in common: the dependence of redshift identification on the existence of the Ly α emission line.

Many different types of objects have been put forward as possible PG candidates, ranging from high-redshift radio galaxies to Ly α emitters found around quasars and damped Ly α systems. Most recently, two promising candidates were announced in the literature. One was the ultra-luminous IRAS galaxy 10214+4724 at $z = 2.29$ (Rowan-Robinson et al. 1991). However, recent observations (Matthew et al. 1994, Eisenhardt et al. 1996) have clearly shown that gravitational lensing is the culprit behind the very large apparent luminosity; the object is consistent with being similar to low-redshift luminous IRAS galaxies. Another recent object of interest is Hawaii-167, an unresolved object at $z = 2.33$ with strong UV absorption lines, discovered by Cowie et al. (1994) from their K -band redshift survey. Egami et al. (1996) interpret this object as a buried quasar with a host galaxy undergoing a strong burst of star formation. Cowie et al. (1995) recently reported the discovery of many galaxies at $1 < z < 1.6$ with star formation rates in excess of $10 M_{\odot} \text{ yr}^{-1}$. However, these massive star forming galaxies are most likely to be galaxies with an on-going (if episodic) star formation history, and not in their first Gyr of their life time. Hence it appears that a PG candidate that everyone can agree on continues to elude searchers.

From a very simplistic view, an object that is at high redshift, looks like a galaxy, and is identified by spectral features consistent with arising entirely from a large number of young stars

would certainly qualify as a PG candidate. In this paper, we describe the serendipitous discovery of an ultra-luminous galaxy at $z = 2.72$, identified by its absorption-line spectrum which appears to have all of these attributes. The object was observed as part of the CNOC (The Canadian Network for Observational Cosmology) Cluster Redshift Survey (Carlberg et al. 1994; Yee, Ellingson, & Carlberg 1996, hereafter YEC). The most conservative interpretation of the spectrum is that it is primarily due to young O, B, and possibly A stars. With its resolved morphology, galaxy-like surface profile, high redshift, and extremely high luminosity (about -26 mag at rest 1500\AA), this object is consistent with being a L^* galaxy observed within the first 100 Myr since its initial star burst. This object appears to fit every definition of a PG.

In Section 2 we describe the imaging and spectroscopic observations that led to this discovery. Section 3 presents the analysis of the spectra and images. We discuss the implications of the results in Section 4. Our conclusions are summarized in Section 5. In this paper, we use $H_0 = 75$ km s $^{-1}$ Mpc $^{-1}$, and $q_0 = 0.1$ throughout.

2. Observations and Reductions

The CNOC Cluster Redshift Survey (see YEC) was carried out to map the velocity field of intermediate redshift EMSS clusters (Gioia et al. 1990) with the primary goal of determining the global mass-to-light ratio of galaxy clusters out to large radii. The project obtained redshifts for ~ 2600 galaxies with magnitudes mostly between Gunn $r=18$ and 22 mag. It was in the process of reducing and analysing this large data set that the PG candidate was discovered in the field of the galaxy cluster MS1512+36. In this section, we briefly describe the relevant information of the CNOC observations and data leading to the identification of the PG, and additional follow-up observations.

2.1. CNOC Imaging and Spectroscopy

The EMSS cluster MS1512+36 at $z=0.373$ (see Gioia & Luppino 1994) was observed at the 3.6m Canada-France-Hawaii Telescope (CFHT) on 1993 June, using the MOS arm of MOS/SIS (Multi-Object-Spectrograph/Subarcsecond-Imaging-Spectrograph, see Le Fèvre et al. 1994). A detailed description of the observing procedure and imaging and spectroscopic data reduction techniques for the survey is presented in YEC. A complete data catalog for this particular cluster is presented in Abraham et al. (1996).

Images of MS1512+36 in Gunn r and g were taken using MOS in the imaging mode with the 2048×2048 LORAL3 CCD on 1993 June 18. The scale of the images is $0.3128''$ per pixel. The integration time of 900 seconds and seeing of $0.9''$ provided a $5\text{-}\sigma$ detection limit of about 24.0 mag for both filters. Photometry for objects in the field was performed using the program PPP (Yee 1991, also see YEC). Calibration to the Gunn system was done using only 3 standard stars,

giving a systematic uncertainty of about 0.07 mag.

Multi-object spectroscopy of galaxies in the field was obtained using slit masks designed from the r image. Two exposures of 60 minutes each were taken on 1993 June 19. For the CNOC program, we were primarily interested in the cluster galaxies; hence, band-limiting filters tuned to the major absorption features of the cluster galaxies were used to shorten the spectra to increase the multiplexing capability of MOS. For MS1512+36 the Z4 filter (see YEC), optimized for clusters with redshift between 0.37 and 0.45, was used. This filter has a spectral range of 4700 to 6300Å. The average dispersion of the O300 grism is about 3.45Å per pixel, providing a resolution of $\sim 16\text{Å}$ with a $1.5''$ slit width. The slits were oriented EW. Spectral reduction and cross-correlation techniques used to extract spectra and obtain galaxy redshifts are described in detail in YEC.

2.2. The Candidate Object

Along with cross-correlation, each spectrum was also examined by eye to double-check the validity of the redshifts and to inspect visually objects for which no redshift is obtained. One object, designated spectroscopically as 1512-cB58 (the 58th spectrum of the B mask in the central field), or PPP#101120, in the field of the cluster MS1512+36, yielded a relatively high signal-to-noise ratio spectrum with a large number of strong absorption lines, none of which correspond to the usual lines seen in optical spectra of moderate-redshift galaxies. The discovery spectrum of this object is presented in Figure 1.

Inspection of the image of the object indicates that it is clearly a galaxy, with a relatively bright r magnitude of 20.5 and situated only $6''$ from the brightest cluster galaxy (BCG) of MS1512+36. Figure 2 shows the central section of the V image taken subsequently with SIS (Subarcsecond-Imaging-Spectrograph) at CFHT (see Section 2.2) with the galaxy cB58 marked. Enlargements of the PG candidate are shown both as a gray scale and a contour plot in Figures 3a and 3b.

Analysis of the spectrum identified 9 lines in the ultraviolet corresponding to an absorption system at $z = 2.72$. These lines are marked on the spectrum in Figure 1. The high redshift, large luminosity, and the resolved nature of the image all indicate that this is a highly unusual object.

2.3. SIS Imaging and Spectroscopy

Because of the remarkable nature of cB58, director's discretionary time at CFHT was requested in 1995 July to obtain further images and spectroscopy of the object. The primary objective was to obtain longer wavelength coverage, including the vital Ly α region, and higher quality images. These new observations were carried out using the SIS arm of MOS/SIS, which provides tip-tilt correction capability and small pixel sampling ($0.0869''$ per pixel) to achieve the

best possible image quality.

Images in Johnson I and V were obtained on 2 separate runs (1995 July 5 and 19). Because the primary purpose for taking the images was for making slit masks for spectroscopic observations, they are not very deep. During each night, exposures of 300 and 600 seconds in I and V , respectively, were obtained. The seeing was $0.64''$ and $0.73''$ FWHM, for the averaged I and V image, respectively. A single standard star field was obtained for each of the nights (NGC7006 for 1995 July 5 and NGC 7790 for 1995 July 19; see Christian et al. 1985). However, because the images from 1995 July 5 were obtained under non-photometric conditions, the photometry is calibrated to that of 1995 July 19.

Spectroscopic observations were made 1995 July 6 using the V150 grism which gives a dispersion of approximately 4.0\AA per double-binned pixel. Two exposures of 40 minutes each were obtained. A slit of width $0.8''$ was used, providing a resolution of about 15\AA . Due to position angle constraints of other programs being carried out on the same night, the slit was oriented north-south, along the minor axis of the galaxy.

The spectrum, shown in Figure 4, was extracted and reduced using IRAF⁸. Extraction was performed using variance-weighting, and the spectrum was wavelength calibrated using vacuum wavelengths of a HeNeAr arc spectrum. Residuals from the calibration solution are $\sim 1\text{\AA}$. The spectrum was flux calibrated and extinction corrected using an observation of the spectroscopic standard BD +40 4032. The flux calibration is estimated to be accurate to about 15% at the ends of the spectrum, and about 10% in the center. However, since the spectrum was taken with a very narrow slit, these uncertainties are lower limits with regard to true spectrophotometry.

3. Analysis

3.1. Spectroscopy

The absorption line features in both spectra were identified and measured using the method described in Bechtold (1994). The observed wavelengths of the lines, along with their rest equivalent width, identification, and redshift, are presented in Tables 1 and 2 for the MOS and SIS spectrum, respectively. The lines are marked on Figures 1 and 4.

To determine the redshift, the CIV $\lambda 1550$ line is not used because of its P-Cygni profile (see below). Using the 8 lines from the MOS spectrum, an average redshift of 2.7233 with a dispersion of 0.0014 is obtained. The rms of the mean is 0.0005. With 9 lines from the SIS spectrum, (discarding also the Al III $\lambda\lambda 1855, 1863$ lines which are in the atmospheric absorption A band), a redshift of 2.7229 with a dispersion of 0.0027 is found. The redshifts determined from the

⁸IRAF is distributed by the National Optical Astronomy Observatories, which is operated by AURA Inc. under contract with NSF.

two spectra are entirely consistent within their errors. We also determined the redshift using an artificial template with the absorption lines (excluding C IV $\lambda 1550$) represented as delta functions. A redshift of 2.7233 is derived from the SIS spectrum, in complete agreement with that obtained by measuring individual lines.

In both spectra, the centroid of the C IV $\lambda 1550$ lines have a redshift about 3.5σ lower than that of the mean redshift of the other lines. This is not the effect of blended lines, as using either 1548 or 1551 Å as the rest wavelength does not alleviate the discrepancy. This shift is most likely due to the line having a P-Cygni profile, which is apparent in the higher signal-to-noise ratio MOS spectrum (Figure 1). The MOS spectrum also shows significant variations in the spectral line widths. For lines that are not blended, most notable are the differences between C II $\lambda 1334$ and Si II $\lambda 1527$, which are interstellar lines, and Si IV $\lambda 1403$ and Al II $\lambda 1671$, which could have a dominant stellar component.

3.2. Imaging

The magnitudes of cB58 in the 4 filters and their estimated uncertainties are listed in Table 3. Also listed are the magnitudes corrected to the AB system (using the calibrations of Fukugita, Shimasaku, & Ichikawa 1995), so that each band has an identical zero point. Because of the crowded nature of the field immediately surrounding the PG, care was taken to derive the correct relative colors of the object. For each filter, an aperture of $2.2''$ diameter centered on the object is used as the object aperture. This size, while large compared to the seeing disk, is small enough to avoid contamination from the cD galaxy and also to ensure the best signal-to-noise ratio possible. The outside diameter of the sky aperture is chosen to be $9''$ in order to avoid the center of the cD galaxy. The $2.2''$ aperture magnitudes are then corrected to total magnitudes using the isophotal surface photometry out to 24.1 mag arcsec² – essentially the faintest contour of Figure 3b. The correction amounts to -0.24 mag. It is not possible to perform photometry to fainter isophots without significant uncertainty being introduced by the halo of the cD galaxy. The uncertainties listed in Table 3 include contributions from both calibration and sky level estimates. The former ranges from 0.07 to 0.1 mag, and the latter contribute a similar amount mainly due to the relatively large uncertainty produced by the proximity of the cD galaxy. At V , which is approximately rest 1500 Å, the absolute magnitude is -26.0 , making this the most luminous non-AGN galaxy ever observed.

The image of the galaxy shows a relatively flat central region with no indication of a central unresolved source (see Figure 3). We can set a limit on the existence of a possible point source by subtracting the brightest point-spread function (PSF) allowed which does not create a central dip in the light distribution of the galaxy. For the summed V image we obtain an upper limit of 22 mag, or about $<25\%$ of the total galaxy light. However, the lack of observable Ly α or other emission or a color gradient (see below) make it unlikely that even this amount of light can arise from an AGN or quasar component.

Profiles of the galaxy in V and I are obtained using the SIS images, which have better seeing and better sampled pixels than the MOS images. To increase the signal-to-noise ratio, the data from the 2 nights are summed, and the pixels are binned 2×2 (which still provides a FWHM of 3.5 or more pixels). The profiles are computed using an isophotal method. Because of the proximity of the BCG of the foreground cluster, the profile is measured only to relatively bright magnitudes.

Isophotal contours separated by a factor of $\sqrt{2}$ in surface brightness are fitted to ellipses. The fitting shows that cB58 has a remarkably regular morphology, confirming the impression from the contour plot. There is essentially no change in the position angles of the ellipses (varying by less than the measurement precision of a few degrees), nor is there evidence of shifting in the centroids of the ellipses with increasing radius (constant within $0.15''$). The only significant change with radius is the ellipticity ($1 - b/a$, where a and b are the semi-major and -minor axis, respectively) which varies from 0.5 at a radius of $1.2''$ for the major axis (at $\sim 4 \times$ seeing disk) to 0.34 at the edge of the galaxy (major axis radius $1.8''$). This change as a function of radius is not due to seeing, as the galaxy isophots become rounder at larger radii. This may be an indication of a more spheroidal system surrounding an inclined disk.

The V and I surface brightness profiles are presented in Figure 5. The radius plotted is that of a circle having the same area as the ellipse (i.e., the harmonic mean of the major and minor axes). Also plotted is the V profile of the PSF from a star $35.1''$ from the galaxy, shifted to show the maximum possible PSF that can be subtracted from the PG without leaving a negative gradient towards the center. The I band profile does not extend as far as the V band because of larger contamination from the cD galaxy in the redder band.

The profiles are fitted to both an exponential disk and a de Vaucouleur law, using data outside a $0.5''$ radius, avoiding the central part which is smeared significantly by the seeing disk. The exponential fits for both the V and I profiles are shown as dashed lines in Figure 5, while the de Vaucouleur fit for the V profile, plotted versus $r^{1/4}$, is shown in Figure 6. Using the V band image, for which we have more extensive data, the exponential fit is clearly superior, with a reduced χ^2 of 0.9, five times smaller than the reduced χ^2 of 5.0 from the de Vaucouleur fit. However, we note that if we also eliminate the third point from the center in the V profile (which may still be contaminated by PSF smearing), the de Vaucouleur law is quite acceptable. Hence, although the exponential disk is a better fit, without higher resolution HST images, we cannot rule out that the galaxy profile is also consistent with a de Vaucouleur law.

The best fitting exponential law has a scale length of $r_o=0.37''$, and a central surface brightness $u_V(0)=20.4 \text{ mag arcsec}^{-2}$. The fitted r_o translates to 2.8 kpc at $z = 2.72$. Assuming it is a circular disk, the deprojected scale length is ~ 3.5 kpc, typical of present-day luminous disk galaxies. The I profile gives an identical scaling length for the exponential fit with $r_o = 0.36''$, indicating that there is no observable color gradient. Dividing the 2-dimensional images of V and I band pixel by pixel confirms the lack of significant color gradients or patchy color differences.

4. Discussion

4.1. cB58 as a Protogalaxy

The extended nature, regular morphology, and the lack of a significant point source or emission lines rule out the possibility that cB58 is a quasar or a quasar-like object. Furthermore, the lack of color gradients and the fact that the absorption lines appear across the whole spatial extent of the spectral images allow us to eliminate the possibility that we are observing the continuum of a background quasar with the absorption lines being produced by an extended (foreground) galaxy at $z = 2.7$. Hence, both the continuum and the absorption lines must arise from a single object.

The strong continuum and absorption lines can be most conservatively be interpreted as arising from early type O, B, and possibly A stars. The spectrum is best compared to the IUE star library in Fanelli et al. (1992) and Kinney et al. (1993), and the IUE spectral atlas of galaxies in Kinney et al. In particular, the spectrum bears a striking resemblance to IUE spectra of starbursting galaxies such as NGC7552 and others in Kinney et al. However, the ultra-violet continuum of cB58 is many hundred times brighter than those of nearby starburst galaxies.

The absorption features in the spectrum can be attributed to both stars and the interstellar medium (e.g., see Kinney et al. 1993; and Leitherer, Robert, & Heckman 1995, here after LRH, for a detailed discussion). Strong stellar lines include Si IV λ 1403, C IV λ 1550, and N IV λ 1720 from O stars, and Al II λ 1671 and Al III λ 1855,1863 from A stars. Dominant interstellar lines include Si II λ 1260, O I+Si II λ 1303, C II λ 1334, Si II λ 1527, C IV λ 1550, Fe II λ 1608, and Al II λ 1671. Massive hot stars develop strong stellar winds with velocities up to 2000 to 3000 km s⁻¹. Hence, it is expected that lines predominantly arising from hot stars are broader than those from the interstellar medium. Although our spectral resolution is relatively poor (~ 900 km/sec), the widths of the strong stellar lines are consistent with being produced by massive hot stars. For example, Si IV λ 1403 and C IV λ 1550, strong lines associated with O stars, are significantly broader than C II λ 1334 and Si II λ 1527, lines that are attributed primarily to the interstellar medium. In both spectra both the line shape and the shifted centroid of the C IV λ 1550 line are strong evidence for the classic P-Cygni profile expected from early O stars. The lack of an emission line at Ly α is consistent with starburst galaxies and HII regions seen locally (Hartman et al. 1988).

The morphology and the exponential profile of the optical image indicate that the object is galaxy-like, with a linear size of ~ 25 kpc. The scale length of ~ 3.5 kpc is entirely consistent with typical L^* galaxies. The smooth light distribution, the lack of measurable color gradients or significant morphological distortion, and the extended nature of the absorption line in the long-slit spectrum all indicate that the young stars are distributed relatively uniformly over the whole object, and that the starburst activity is not localized.

The high luminosity and global nature of the starburst activity argue that this galaxy most likely has very recently undergone a starburst which is massive enough to be the initial burst

associated with the formation of this galaxy. In the following sections, we examine in more quantitative detail this interpretation and its implications.

4.2. Models

Constructing detailed and definitive models of the star formation history of a galaxy is difficult, even at such a young age. There are many uncertainties in input parameters for this type of modeling; e.g., initial mass function (IMF), metallicities, and the nature of dust. These uncertainties are greatly accentuated because the PG is being observed at a time when the universe is expected to be very different from the present. Nevertheless, the current data, though limited, allow us to set interesting limits on some of the parameters.

For any star forming galaxy, three basic components are usually required for modeling: an existing population of stars, on-going star formation, and dust. Each of these components has many parameters which are not well constrained. And often, depending on the data on hand, some important parameters are degenerate. For instance, it is often not possible to separate the effects of stellar age and dust using colors.

For first order modeling of the stellar population of the galaxy, we compare the broadband photometry with the spectral energy distributions (SEDs) from GISSEL models of Bruzual & Charlot (1993). The range of models are then investigated in more detail in conjunction with the spectroscopic data. It should be noted that such modeling can only be considered as approximate, as it is certain that young galaxies at these redshifts will not have the near-solar metal abundance on which these models are based.

We have not used the continuum of the SIS spectrum for SED model fitting because of uncertainties in the fluxing. However, we note that the SIS spectrum agrees with the g , V , and r photometry very well, although it differs by about 25% (too bright) at I . The discrepancy in I is probably the result of light loss in the calibration standard star due to the narrow slit used; such a loss may have been much less severe for the resolved galaxy. The accuracy of the photometry is verified by comparing data from 3 cluster galaxies (at $z = 0.373$) to the SEDs of evolved galaxies from Bruzual & Charlot (1993).

For dust extinction, we use a slightly modified version of the average LMC extinction curve from Fitzpatrick (1986). We have interpolated over the 2175Å hump in the LMC extinction, based on the fact that in red end of the SIS spectrum, which are equivalent to 2200Å rest, we see no evidence for the expected prominent dip due to this feature. We note that many local star burst galaxies do not show this bump in the extinction in their IUE spectra also (Kinney et al. 1993).

Figure 7 shows a comparison of single starburst models from Charlot & Bruzual (1993) and the broad-band colors, which have been corrected for differing amounts of extinction. Unfortunately, extinction and stellar age are degenerate in modeling the colors. Assuming that there is no dust,

the optical photometry indicates a single-burst model at an age of about 400 Myr. This can then be considered as the upper limit of the age of the star formation, and will be referred to as the *400-Myr model*. We note that these results are based on the “standard” GISSEL default models with an upper mass cut-off of $125 M_{\odot}$; changing this cut-off does not affect any of the conclusions based on the SED.

As more extinction is added, younger ages fit the data better. The spectral energy distribution can be fitted by an arbitrarily young model up to an extinction of about $E(B - V) \sim 0.4$, beyond which the SED is definitely too steep even for the hottest stars. Figure 7 also shows two models with extinction corrections. For $E(B - V) = 0.18$, the best fitting age is 200 Myr. As an example of a very young model, using $E(B - V) = 0.3$, the data fit an age of 5 Myr or less.

Within our observational error bars, models for constant star formation essentially look identical to the very young single-burst model at these wavelengths. Figure 8 shows the comparison of constant star forming models and the data with an extinction correction of $E(B - V)=0.3$. In the observed optical bands, the SED is not able to distinguish models of ages between zero and 500 Myr. Observations in the near-IR bands should be able to set an upper limit to the age of the constant star formation models. We note that a SED with less extinction will not fit any of the constant star formation models. We shall refer to the dusty young extremes of these models as the *single-burst young model* and the *constant formation young model*, or generically as the *young models*. We note that for all the models discussed so far, an additional much older population, if it exists, does not contribute significantly to the flux at the observed optical bands. In the following, we discuss the models in more detail.

The 400-Myr model fits the UV SED very well. The smooth appearance of the galaxy and the lack of color gradients are consistent with the low dust content required by this model. However, this limiting model has a number of serious problems. First, we note that assuming a standard IMF, this model is expected to fade to an evolved galaxy of about -25.3 mag in V (rest), or about $25L^*$, a highly improbably luminosity for a present-day galaxy, even for a BCG. The ancestor of such a rare galaxy would have an extremely low probability of being discovered in our survey (see Section 4.3). We note that somewhat younger (e.g. 200 Myr) single-burst models suffer from the same problem. The increase in luminosity from the extinction correction negates most of the compensation from the larger fading expected from the younger age. A flatter IMF, or a low-mass cut off which may have been seen in some low-redshift starburst galaxies (e.g., see Charlot et al. 1993), could lower the expected evolved rest V band luminosity. Preliminary K band photometry (to be reported in a future paper) may be consistent with such a scenario.

A more immediate problem is based on the spectroscopic data. The 400-Myr model, or any single-burst models older than about 10 Myr, cannot explain the entire stellar population. Our spectra show strong evidence of P-Cygni profile in C IV $\lambda 1550$ arising from massive winds from early O stars. Hence, star formation must be on-going or has stopped less than 10 Myr ago, and either scenario must have a significant effect on the UV continuum.

The young models are favored by the the existence of CIV P-Cygni profile. The depth of the broad absorption component of CIV $\lambda 1550$ and the height of the emission component are qualitatively consistent with line profiles of starburst models in LRH. Since the 3 parameters of age, IMF slope, and upper mass cut-off are correlated, a number of combinations of these 3 parameters produce profiles that are similar to the observed one. In particular, two continuous formation LRH models strongly resemble our line profile: one has a Salpeter IMF with an upper mass cut-off of $40 M_{\odot}$, and the other has a steeper IMF slope (3.0) with an upper mass cut-off of $80 M_{\odot}$. Both have an age of 9 Myr or greater (at which time the creation and death of massive O stars come into equilibrium). In Figure 9 we plot the CIV $\lambda 1550$ profile from the MOS spectrum overlaid by the model profile having a Salpeter IMF with an upper mass cut-off of $40 M_{\odot}$. The agreement is excellent. Models that are significantly younger, with flatter IMFs, or having more massive upper mass cut-offs, have too large P-Cygni profiles; while models that are steeper in the IMF or lower in upper mass cut-off have too small profiles.

Similarly, we find that for the single-burst scenario, the line profile is well-described by models with ages of between 5 to 7 Myr for the whole range of IMF slopes and upper mass cut-offs in the LRH models. We note that “single-burst” star formation is not physical, but is used as a description for a relatively short star formation episode that has already stopped at the time of observation. As an illustration, in Figure 9 we also plot a LRH model with the standard IMF and an upper mass cut-off of $80 M_{\odot}$ at an age of 8 Myr after a single star burst. It clearly does not fit the observed profile, indicating that star formation could not have stopped completely for more than 8 Myr.

The constant star formation and single-burst models in theory can be distinguished by the Si IV $\lambda 1394, 1402$ lines. According LRH, the 5 Myr single-burst models should have relatively stronger P-Cygni profiles than the constant star formation models, due to enhancement from supergiants in the former. The Si IV lines in the PG spectrum are heavily dominated by interstellar contributions. There is a possible indication of an emission component of a P-Cygni profile in the Si IV $\lambda 1403$ line; however, there is no evidence of a blue broad wing from the Si IV $\lambda 1394$ line. This may indicate a preference of the continuous star formation models over the very young single-burst models. Higher quality data are required for a more definitive conclusion. However, we note that based on a probability argument, it is not highly plausible that we would observe this galaxies within such a short time since its cessation of star formation.

Although the CIV P-Cygni profile appears to be in agreement with some LRH models, a strong caveat is that they are based on solar metallicity. Hence, these results should not be taken too literally, but rather as indicative. For lower metallicity massive stars, it is expected that the stellar winds will be less strong due to fewer C^{3+} ions. Hence, qualitatively, the upper cut-off mass could be higher, the IMF could be flatter, or the age could be younger. We also note that if there is a significant additional underlying continuum, the intrinsic P-Cygni profile would be larger relative to the true young star continuum.

For the young models, we can use the 1500Å continuum to estimate the star formation rate based on the models of LRH. The observed V (which is equivalent to almost exactly 1500Å rest) magnitude of 20.6 corresponds to a luminosity of 4.3×10^{42} erg s⁻¹Å⁻¹, assuming no dust correction. Depending on the upper mass cut-off and the slope of the IMF, LRH predict 1500Å luminosities between $10^{38.95}$ to $10^{40.6}$ ergs s⁻¹ Å⁻¹ at an age of 9 Myr for a constant star formation rate of 1 M_⊙ yr⁻¹. Taking a value of $10^{40.04}$ ergs s⁻¹ Å⁻¹ (for a model with standard IMF slope and a 40 M_⊙ cut off), ignoring extinction for the time being, and attributing all of the observed V luminosity to the constant star forming component, we obtain a star formation rate of ~ 400 M_⊙ yr⁻¹. This rate can be considered as a very generous upper limit for any on-going star formation in a dust-free model. For the constant star formation young model, the flux at 1500Å has to be corrected for extinction by a factor of about 12.4, implying a star formation rate of 4700 M_⊙ yr⁻¹. Since a typical L^* galaxy has a stellar mass of $\sim 5 \times 10^{10}$ M_⊙, a galaxy forming stars at this rate will assemble into a relatively massive $2L^*$ galaxy of 10^{11} M_⊙ in stellar mass in about 20 Myr. However, it should be remembered that the 1500Å luminosity is highly dependent on the parameters used in the star formation model. For example, with a flatter IMF slope of 1.5 and an upper mass cut-off of 80 M_⊙, the star formation rate can be lowered by a factor of 3.6, requiring about 75 Myr to build up a 10^{11} M_⊙ galaxy. This sets the range of the age of the galaxy in a constant star formation model to be on the order of 10 to 100 Myr.

Similarly, we can apply the LRH models to estimate the size of a young single-burst model. For a single burst of 10^6 M_⊙ yr⁻¹, the 1500Å luminosity is $10^{39.0}$ erg s⁻¹Å⁻¹ for the standard LRH model (Salpeter IMF and upper mass cut-off of 80M_⊙) at an age of 7 Myr. Using the observed 1500Å luminosity, the size of the single burst is estimated to be 4.3×10^9 M_⊙, assuming no extinction. The continuum again must be corrected by a factor of 12.4 for extinction for the young single-burst model, bringing the burst strength to 5.3×10^{10} M_⊙. Thus, for the young single-burst model, the star formation from the burst alone amounts to about a L^* galaxy.

In both cases the young models allow the galaxy to be observable relatively easily for about 5 to 10 Myr after the end of star formation, at which time the observed V band photometry will drop by about 1 to 2 mag. Using the extinction required and the K-correction from GISSEL models and assuming passive evolution from the time of observation, we estimate that the single-burst formation model will produce an evolved galaxy about 7 mag fainter in rest V , creating a present-day galaxy with an absolute rest V magnitude of -21.4, or about $1.7L^*$. This luminosity is consistent with the mass from the estimates of the star formation rate.

Although it appears that the young models afford very reasonable fit to both photometric and spectroscopic data, there are, however, a few difficulties that need to be addressed. Several problems are related to the short time scale expected for cB58 to build up a relatively massive galaxy, especially for the lower end of the age range of 10 to 20 Myr. First there is the problem with the creation of metals that we see so prominently in the spectrum. Although this can be explained by postulating a much fainter (at 1500Å) older component that is completely hidden by the new star formation, such a model would require the present-day descendant of this galaxy to

be even more luminous. Second, the relatively smooth morphology and lack of color gradients also argue against such a young age. It is difficult to imagine such homogeneity in a galaxy after only about 10 Myr into its initial star formation, since the typical dynamical time for a sizable galaxy is about 10^8 yrs. We note that both of these problems can be potentially alleviated by the flat IMF models, which have star formation rates such that it will take about a 100 Myr to assemble a massive galaxy.

The young models are also not consistent with all of the observational data. First, although the observed SED fits the young models reasonably well, it is discrepant at the blue end at the 2σ level. A huge on-going star burst produces a very steep blue continuum with $F_\lambda \sim \lambda^{-2.5}$. The observed continuum is essentially flat around 1500\AA with a roll-over around 1300\AA . The roll-over is seen in both the fluxed SIS spectrum and the $g - r$ color. The standard dust extinction curve is not able to reproduce the steep continuum shape required by a young model at the g band without having to resort to additional absorption beyond 1300\AA . However, we note that the amount of extra extinction required is within the uncertainty in the standard extinction curve. Second, there is some evidence that that O stars may not completely dominate the continuum light. In the spectrum, a strong AlII $\lambda 1671$ absorption line is seen. This line likely has a significant stellar component as it is broader than the pure interstellar lines, such as CII $\lambda 1334$ (see Figure 1). The AlII $\lambda 1671$ line could be an indicator of a component of early A type stars in the continuum. Additional data in the IR bands may allow us to put a limit on the size of an older component.

Dust is often thought to be associated with forming galaxies or star bursts. It is likely that our PG candidate does not contain an extraordinary amount of dust. The $E(B - V) = 0.3$ required by the young models is not an outlandish amount and is consistent with the average values that are seen towards O star associations in the LMC (LRH). The smoothness of the optical images and the lack of significant color variance argue against significant patchiness due to dust. The lack of Ly α from the HII regions expected from the young stars requires only a small amount of dust as an explanation.

In summary, our optical photometry is able to limit the age of the galaxy to younger than ~ 400 Myr, with the age critically dependent on the extinction correction, which is limited to $E(B - V) < 0.4$. However, the 400-Myr model is highly unlikely because of the object’s very large luminosity. Moreover, spectroscopic signatures of a P-Cygni profile for CIV $\lambda 1550$ require that there be a significant number of O stars, and hence a component that is either forming stars or has an age younger than ~ 10 Myr must exist. Simple standard models over the whole range of ages all have their respective problems, and none appears to be able to explain all the observations so far. This may be an indication of a non-standard IMF or dust absorption law. Such a conclusion is not surprising, as there seems little reason to believe that star formation and dust absorption in a primeval galaxy should operate in a manner identical to those in nearby galaxies. The most likely scenario is that this galaxy is somewhere between 50 and 100 Myr in age, contains a small amount of relatively uniformly distributed dust, and is forming stars at a high rate, probably with a non-standard IMF.

4.3. Estimate of Sky Density

We have shown that we can interpret the galaxy cB58 as an early-type galaxy observed within 100 Myr of its major star formation episode. Is this object the first of a new, but relatively common, class of high-redshift object? How likely is such a galaxy be observed serendipitously? It is of interest to make an order-of-magnitude estimate of the density of such objects on the sky to see if it is probable to expect the CNOC cluster redshift survey to find one.

There are many factors that enter into the detectability of a PG: the volume density, the luminosity, the recognizability of the object (i.e., observable spectroscopic signatures), and the time interval over which these conditions are favorable. We can estimate the expected number of such objects using our knowledge of galaxy density and the observational parameters of the CNOC survey. However, it should be noted that many of the parameters used are highly uncertain.

For an object similar to cB58, there is a relatively small redshift window in which the object is observable. In order for this object to be identified unambiguously, the spectral region that is rich in absorption lines must be in the observed band, especially when this type of object has not been observed before. This spectral region ranges from Si II λ 1260 to Al II λ 1671. Ly α is not included because of the rapid drop in the continuum there. To the red of Al III $\lambda\lambda$ 1855,1863, there are no significant absorption lines up to well past 2000 \AA rest. To be able to detect a similar PG, let us assume that we need to cover the minimum of C IV λ 1550 for the low redshift limit, implying $z \sim 2$. Similarly, we require C IV λ 1550 at the red end of the spectrum for the high redshift limit, implying $z \sim 3$.

The CNOC1 redshift survey covers 0.66 square degrees. The volume between $z = 2$ and 3 subtended by 1 sq deg is about $8.4 \times 10^6 \text{ Mpc}^3$. Using the present date co-moving density of galaxies derived from integrating the luminosity function of Loveday et al. (1993), we expect ~ 1600 galaxies in the volume sampled by CNOC that are as bright as $2L^*$, the expected evolved luminosity of the young models. If we assume that galaxy formation is uniform between $z = 5$ and 2, then approximately 1/2 of all galaxies would be formed in the interval of $2 < z < 3$. Of these 800 galaxies, about 20% may be expected to be early-types with most of their stars formed in a short-duration large burst, reducing the number to 160. These forming galaxies will be in an ultra-luminous phase for only a short period of time. Assuming this to be ~ 50 Myr, then about 1/45 of them will be visible at any one time, bringing the number down to 3.5. The CNOC survey has an average completeness of about 40% between $r = 20$ and 21 mag (mostly due to the many low-redshift clusters in the sample). Hence, the expected number is about 1.5. The interpretation of this object as a PG *can be* consistent with its serendipitous discovery in the CNOC survey. Using the above estimates, we might expect to find between $10^{0\pm 1}$ such galaxies per square degree at magnitudes brighter than $r=21$.

Of course, our estimate contains many uncertainties of a factor much larger than 2 each. Within the extreme range of models that we discussed, there may be a factor as large as 100 introduced in the uncertainty of the sky density. As an example, if we use the 200-Myr single burst

model, the observable life-time is increased by a factor of about 4, but it is more than offset by the factor of over 1000 fewer galaxies expected to be as bright as $10L^*$. Other large uncertainties include the volume sampled, which differs by a factor of 3 between $q_0 = 0.1$ and 0.5, and the fraction of L^* galaxies that were formed at $2 < z < 3$. For instance, if only 10% of L^* galaxies were formed in this redshift period, then we would expect a factor of 5 fewer such objects. If the bulk of these galaxies were formed at higher redshift, a fainter spectroscopic survey further out in the red is required. Also uncertain is the fraction of galaxies that undergo such a huge burst of star formation. It should be noted that, conversely, additional discoveries such as this should allow us to constrain these important parameters. Our order-of-magnitude estimate here is merely to demonstrate that it is not entirely unreasonable for a survey such as CNOC to discover such a PG candidate serendipitously.

4.4. Possible Effects of Lensing

The main thrust of the interpretation that cB58 is a galaxy at the very early stage of its history is its enormous luminosity, and hence star formation rate. Gravitational lensing can cause the luminosity of an object to increase many fold. An example of a PG candidate being lensed, and hence not being as luminous as was first thought, is IRAS10241+4724 (Rowan-Robinson 1991, Broadhurst & Lehár 1995, Eisenhardt et al. 1996) at $z=2.29$. IRAS10214+4724 was first detected in a ground-based image, with substantially poorer seeing ($1.5''$) than ours. However, higher resolution images, both ground-based IR and HST optical images, show that the object is lensed with an estimated brightening of about a factor of 30 to 100 (Eisenhardt et al. 1996). Another example of a lensed high-redshift galaxy is arc #384 of in Abell 2218 with a spectrum similar to cB58 at a redshift of 2.51 (Ebbels et al. 1996), discussed in Section 4.5.

Our PG candidate is $6''$ from the cD galaxy in MS1512+36, a relatively poor (equivalent to Abell richness 0) cluster at $z = 0.373$ with a velocity dispersion of 690 km s^{-1} (Carlberg et al. 1996). The proximity of the BCG to the protogalaxy candidate requires an examination of the possible effect of lensing on the luminosity of the object. However, we note that even a magnification of a factor of several in the luminosity does not severely diminish the interpretation that this object is being observed at a very luminous phase of its life time.

Large magnification usually occurs in the presence of a very strong image shear, as is the case for arcs. Our images of the PG under exceptional ground-based seeing show no sign of distortion, and hence is very unlikely that it is being strongly sheared, or multiply imaged. Any lensing similar to that seen in IRAS10241+4724 would have been easily detected in our V image with $0.65''$ seeing. The axes of the galaxy are neither tangential nor radial with respect to the center of the cD galaxy, which again argues against the possibility of strong lensing. In addition, an examination of both our images and the deep image in Gioia & Luppino (1994) reveals no sign of other gravitationally lensed arcs near the cluster. Based on the axis ratio of the galaxy of < 2 and the very smooth and regular morphology of the object, an upper limit of a magnification of 2

from weak lensing can be established. Such a low upper limit does not change the conclusion with regard to the high luminosity of the galaxy.

The fact that this object is completely resolved in both directions is the primary argument against gravitational lensing. However, it is possible, although very unlikely, that strong magnification can result without shear. This can occur when there are two subcritical lenses superposed in such a way that the image lies at a location where the shear of one lens is at right angles to the shear of the other. In particular, if the cD is off-center and outside the critical radius of the cluster, then in the directions perpendicular to the cD-cluster center line there will be two positions of considerable magnification, but with little image shear. An alternate possibility is that if the cD and cluster potential have a common center (at least in projection), then a subcritical cluster without a central cusp has a small zone of large magnification, close to the cD and with little image shear and no counter images. (L. Williams, private communication). In both cases a very precise alignment of two lensing mass profiles possessing a narrow range of parameters is required. At this point, we cannot rule out these possibilities, despite the low probability. However, the poorness of the cluster probably precludes a very large lensing magnification even if the geometry is satisfied.

4.5. Comparison to Other Objects at High z

Most objects found at high redshift have been discovered as a result of their non-stellar radiation. These include quasars, high-redshift radio galaxies, and IRAS galaxies. They are typically identified by emission lines, especially $\text{Ly}\alpha$, and stellar spectral signatures have been difficult to observe. Another major class of objects that are inferred to be at high redshift are the objects responsible for the quasar absorption lines; however, little is known about their stellar content.

The object bearing a close spectral resemblance to cB58 is Hawaii-167 at $z = 2.33$, discovered by Cowie et al. (1994). This object was observed as part of their deep K -band survey. The optical spectrum shows strong absorption lines in the UV, similar to cB58, and the I band magnitude is nearly identical. However, the similarities end here, and there are major differences. Foremost is that Haw167 is unresolved. Furthermore, it is much redder in the optical: $B - I \sim 3$ mag for Haw167 vs $g - I = 0.7$ mag. (Note that B at $z = 2.33$ is identical in rest wavelength to g at $z = 2.72$.) This color difference is borne out by the drop at about 1800\AA rest in the spectrum of Haw167, which is not found in cB58. Egami et al. (1995) interpret Haw167 as a dust-enshrouded QSO with a star burst. Morphologically cB58 is clearly not a quasar, and the difference in color may be due to either dust or a somewhat older stellar population in Haw167.

Cowie et al. (1995) have also discovered a significant population of strong $[\text{O II}]\lambda 3727$ galaxies at z between 1 and 1.7. They interpret these as massive star forming galaxies with a star formation rate of $> 10M_{\odot} \text{ yr}^{-1}$. It is unlikely that cB58 is a member of this population. More likely, the

objects found by Cowie et al. represent continuous star forming galaxies, (hence, probably later morphological types), whereas cB58 may be representative of galaxies with a massive initial burst of star formation creating most of the stellar mass.

Recent observations of arcs in Abell 2218 have discovered one at $z = 2.51$ with an absorption-line spectrum (Ebbels et al. 1996). This arc has a spectrum that resembles very closely that of cB58, but with weaker absorption features. However, the intrinsic luminosity of this lensed galaxy is several magnitudes fainter than cB58 (Kneib et al. 1996), hence, this galaxy is most likely undergoing a more minor star-burst.

5. Summary

We have serendipitously discovered an excellent protogalaxy candidate at $z = 2.72$ from the CNOC redshift survey. Images in four different filters under excellent seeing show that it is well resolved with a surface profile consistent with an exponential law with $r_o \sim 3.5$ kpc. Modeling the SED sets an upper limit of 400 Myr as the age of the stellar population, with arbitrary younger ages possible when the continuum is corrected for dust extinction. The strong absorption-line spectrum, including the existence of a prominent P-Cygni profile in CIV $\lambda 1550$, requires a dominant component with massive on-going star formation. Comparison with starburst models indicates that the spectroscopic data are consistent with either a continuous star formation model with a star formation rate of several thousand M_\odot per year, or a 5 to 10 Myr old single-burst massive enough to have formed a L^* galaxy. The lack of morphological peculiarity or a significant color gradient indicate that the star formation is not localized, but occurring over the whole galaxy, requiring that the the star formation have been proceeding for a duration close to the dynamical time of the galaxy. The total luminosity of the this object is extremely large, with an observed absolute magnitude of -26 at 1500\AA . Assuming either the single-burst young model or the constant star formation model, we expect this object to evolve into a galaxy equivalent to $\sim 2L^*$. Because of the the very large star-formation rate, which can assemble a massive galaxy in 25 to 100 Myr, we prefer to interpret this object as a precursor of an early-type galaxy. At this point, none of the data indicate that the high luminosity arises from gravitational lensing. Additional observations at other wavelengths, both imaging and spectroscopic, with higher signal-to-noise ratios and higher spatial resolution, will allow us to define the star formation history with more certainty.

We estimate the density of such objects on the sky to be $10^{0\pm 1}$ per square degree based on this interpretation. The discovery of one such object in the CNOC cluster redshift survey is statistically consistent with it being a bright early-type galaxy observed at a very young stage. The relatively high sky density expected for such objects suggests that this is a member of a relatively common class of objects in the sky. Additional discoveries and detailed investigations of this type of object will provide immensely important insights and constraints on galaxy formation and evolution.

We wish to thank Pierre Couturier, the director of CFHT, for the generous granting of director's discretionary time to obtain additional imaging and spectroscopy data on this object. We thank Christian Vanderriest for obtaining some of the SIS images. We would also like to thank Peter Conti, Norm Murray, Mike Shull, and Liliya Williams for useful discussions. RGC and HKCY acknowledge NSERC for financial support. EE acknowledges NASA grant NAG-5-2896 and an NOAO travel grant. JB is supported by NSF grant AST-9058510. HKCY is grateful for the hospitality offered by CFHT, where part of the manuscript was prepared.

REFERENCES

- Abraham, R.G., Yee, H.K.C., Ellingson, E., Gravel, P., Carlberg, R.G., Pritchett, C.J. 1996, preprint to be submitted to ApJS.
- Bechtold, J. 1994, ApJS, 91, 1
- Bruzual, G.A. & Charlot, S. 1993, ApJ, 405, 538
- Broadhurst, T.J. & Lehar 1995, AJ, 102, 1956
- Carlberg, R.G., et al. 1994, JRASC, 88, 39
- Carlberg, R.G., Yee, H.K.C., Ellingson, E., Abraham, R.G., Gravel, P., Morris, S., & Pritchett, C.J. 1996, ApJ, in press
- Charlot, S., Ferrari, F., Mathew, G.J., & Silk, J. 1993, ApJL, 419, L57
- Christian, C.A., Adams, M.T., Barnes, J.v., Butcher, H.R., Hayes, D.S., Mould, J.R., & Siegel, M.J. 1985, PASP, 97 363
- Cowie, L.L., Songaila, A., Hu, E.M., Egami, E., Huang, J.S., Pickles, A., Ridgway, S.E., & Wainscoat, R.J. 1994, ApJ, 432, L83
- Cowie, L.L., Hu, E.M., & Songaila, A. 1995, Nature, 377, 603
- Djorgovski, S. 1992, in *Cosmology and Large-Scale Structure* ASP Conference Series, 24, 73
- Djorgovski, S., Spinrad, H., McCarthy, P., & Strauss, M.A. 1985, ApJL, 299, L1
- Ebbels, T., LaBorgne, J.-F., Pello, R., Kneib, J.-P., Ellis, R.S., Smail, I., & Sanahuja, B. 1996, in preparation
- Egami, E., Iwamuro, F., Maihara, T., Oya, S., & Cowie, L.L. 1995, ApJ, in press
- Eisenhardt, P.R., Armus, L., Hogg, D.W., Soifer, B.T., Neugebauer, G., Werner, M.W. 1996, ApJ, in press
- Fanelli, M.N., O'Connell, R.W., Burstein, D., & Wu, C.-C. 1992, ApJS, 82, 197
- Fitzpatrick, E.L. 1986, AJ, 92, 1068
- Fukugita, M., Shimasaku, K., & Ichikawa, T. 1995, PASP, 107, 945

- Gioia, I. M., Maccacaro, T., Schild, R. E., Wolter, A., Stocke, J. T., Morris, S. L., & Henry, J. P. 1990, *ApJS*, 72, 567
- Gioia, I. M. & Luppino, G. A. 1994, *ApJS*, 94, 583
- Hartman, L.W., Huchra, J.P., Geller, M.J., O'Brien, P., & Wilson, R. 1999, *ApJ*, 326, 101
- Kinney, A.L., Bohline, R.C., Galzetti, D., Panagia, N., & Wyse, R.F.G. 1993, *ApJS*, 86, 5
- Kneib, J.P., Ellis, R.S., Smail, I., Couch, W.J., & Sharples, R.M. 1996, preprint
- Koo, D.C. 1986, in *Spectral Evolution of Galaxies*, eds Chiosi & Renzini, page 419.
- Leitherer, C., Robert, C., & Heckman, T.M. 1995, *ApJS*, 99, 173 (LRH)
- Loveday, J., Efstathiou, G., Peterson, B.A., Maddox, S.J. 1993, *ApJ*, 390, 338
- Matthew, K. et al. 1994, *ApJ*, 420, L13
- McCarthy, P. 1993 *ARAA*, 31 639
- Rowan-Robinson, M. et al. 1991, *Nature*, 351, 719
- Pritchett, C.J. 1994, *PASP*, 106, 1052
- Pritchett, C.J., & Hartwick, F.D.A. 1990, *ApJL*, 355, L11
- Steidel, C. & Hamilton, D. 1993, *AJ*, 105, 2017
- Tinsley, B. 1972, *ApJ*, 178, 319
- Wolfe, A.M. 1995, in the Proceedings of the ESO Conference on QSO Absorption Lines, ed.G. Meylan, (Springer-Verlag : Berlin), 13
- Yee, H.K.C. 1991, *PASP*, 103, 396
- Yee, H.K.C., Ellingson, E., & Carlberg, R.G. 1996, *ApJS*, 102, 269 (YEC)

TABLE 1. Absorption Line List (MOS Spectrum)

Wavelength (Å) ±	EW (Å) ±		ID	z	
4693.9	1.4	4.4	0.9	Si II 1260.4	2.7241
4758.0	1.4	2.5	0.4	—	—
4852.9	1.0	5.6	0.4	OI 1302.2, SiII 1304.4	2.7236
4969.0	0.9	3.4	0.3	CII 1334.5	2.7234
5189.6	0.7	2.8	0.2	SiIV 1393.8	2.7234
5221.2	1.3	2.3	0.2	SiIV 1402.8	2.7204
5683.8	0.7	2.4	0.2	SiII 1526.7	2.7229
5761.5	0.5	5.5	0.2	CIV 1548.2, 1550.8	(2.7183)
5992.0	1.3	2.1	0.2	FeII 1608.4	2.7253
6221.4	1.0	2.6	0.2	AlII 1670.8	2.7236

TABLE 2. Absorption Line List (SIS Spectrum)

Wavelength (Å) ±	EW (Å) ±		ID	z	
4522.7	6.1	11.4	2.5	Ly α 1215.7	2.7203
4696.1	4.4	3.0	0.9	Si II 1260.4	2.7258
4848.4	3.1	4.6	0.7	OI 1302.2, SiII 1304.4	2.7201
4963.1	1.9	4.3	0.5	CII 1334.5	2.7191
5112.2	2.4	2.2	0.4	—	—
5187.8	1.6	3.2	0.4	SiIV 1393.8	2.7221
5223.3	2.2	2.2	0.4	SiIV 1402.8	2.7235
5688.2	1.5	3.7	0.3	SiII 1526.7	2.7258
5757.5	1.1	6.1	0.4	CIV 1548.2, 1550.8	(2.7157)
5988.6	2.1	2.6	0.3	FeII 1608.4	2.7232
6225.5	1.7	3.8	0.4	AlII 1670.8	2.7261
6904.8	2.3	5.6	0.4	AlIII 1854.7, 1862	—

TABLE 3. Photometry (3'' aperture)

Band	Magnitude	\pm	AB Magnitude
<i>g</i>	21.08	0.10	21.15
<i>V</i>	20.64	0.12	20.64
<i>r</i>	20.60	0.10	20.41
<i>I</i>	19.92	0.12	20.35

Fig. 1.— Discovery Spectrum of the protogalaxy, plotted in observed wavelengths. Identified absorption lines are marked.

Fig. 2.— Gray scale plot of the central section of SIS image in V of MS1512+36, showing the center of the cluster and the PG. The protogalaxy candidate is marked by the letters ‘PG’. NE is upper-left. Intervals on axes are labeled in arcseconds.

Fig. 3.— (a) Enlarged gray scale plot of the PG in V . (b) Contour plot of the V band image of the protogalaxy to the same scale as the gray scale. Contours are factors of 1.41 apart beginning at the peak pixel. The last contour is 24.1 mag/sq arcsecond.

Fig. 4.— SIS spectrum of the protogalaxy, plotted in rest wavelengths. Identified absorption lines are marked. The spectrum has been smoothed by a box-car filter of 3 pixels in size. Note the lack of an emission line at $\text{Ly}\alpha$.

Fig. 5.— V (top panel) and I (bottom panel) surface profiles of the protogalaxy. Exponential law fits to the outer points are shown as dashed-lines. Also plotted (dot-dashed line) is the PSF from a bright star, scaled to the maximum brightness that can be subtracted from the PG.

Fig. 6.— V profile of the PG but plotted versus radius^{1/4}. The best fitting de Vaucouleur $r^{1/4}$ law is shown as a dashed-line. Note that the exponential law fit is considerably better. However, if only the 5 outer points are used, a $r^{1/4}$ law provides an acceptable fit.

Fig. 7.— Comparison of single-burst star formation models with g , V , r , and I photometry. The bottom set of points are the observed fluxes, with the other two sets of points representing corrected fluxes with extinction of $E(B - V)=0.1$ and 0.3, middle and top, respectively. The horizontal “error-bars” represent the half-width of the filters. Solid lines from bottom to top represent GISSEL models of 400, 200, and 5 Myr after a single burst .

Fig. 8.— Comparison of constant star formation models with g , V , r , and I photometry corrected by an extinction of $E(B - V) = 0.3$. Solid lines from bottom to top represent GISSEL models of constant star formation at ages of 500, 50, and 5 Myr.

Fig. 9.— Enlargement of the MOS spectrum, shown as the thin solid line, around the C IV $\lambda 1550$ region, illustrating the P-Cygni profile. The other strong absorption line is Si II $\lambda 1527$. The thick solid line shows the C IV $\lambda 1550$ profile from the constant star formation model of Leitherer et al. (1995) at 9 Myr with the Salpeter IMF and a 40 M_{\odot} upper mass cut-off. The agreement is excellent, with the PG spectrum showing considerably stronger interstellar components. The thick dashed line shows the model profile at an age of 8 Myr after a single burst with the Salpeter IMF and an 80 M_{\odot} upper mass cut-off. The model clearly does not fit as well and indicates that the upper limit of the age of a single burst is about 7 Myr.

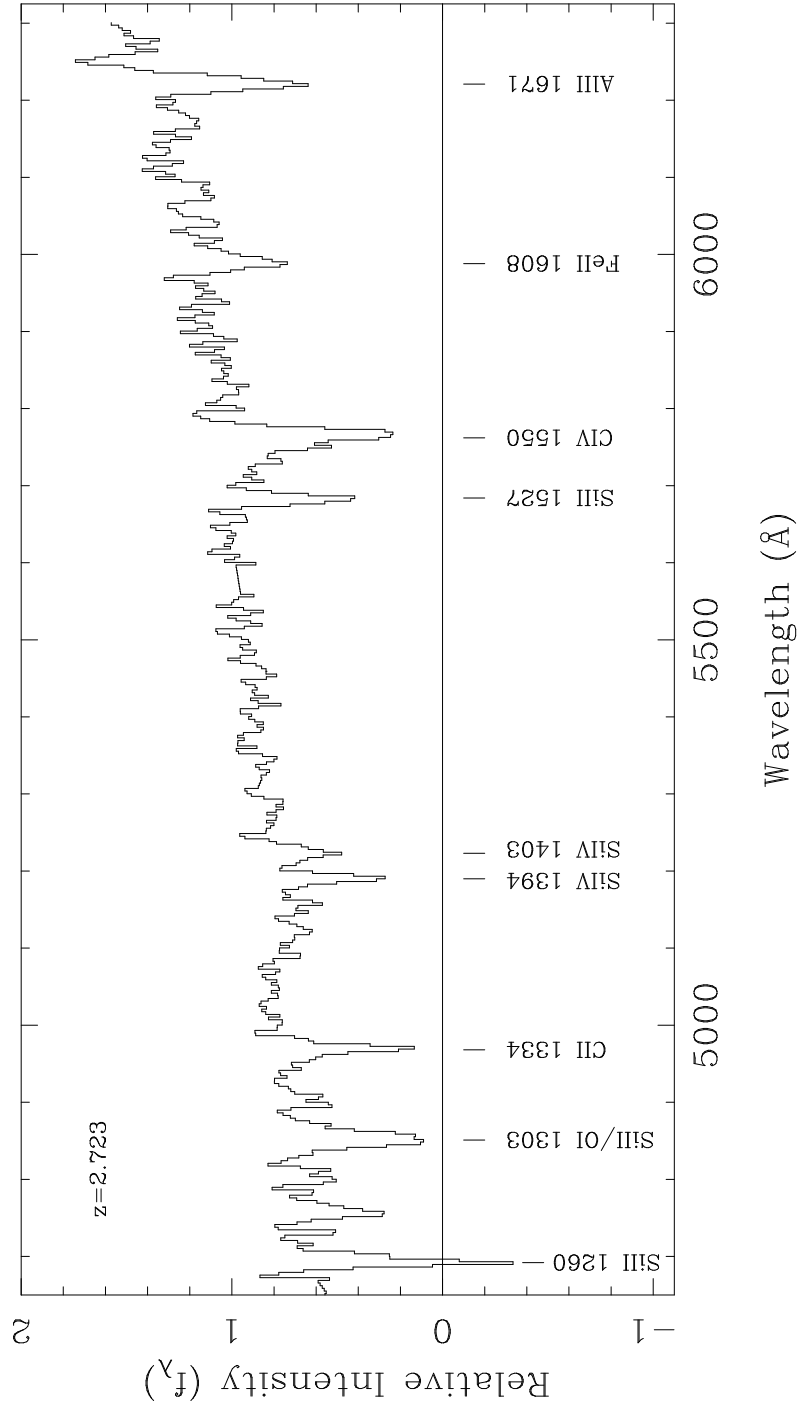


Fig. 1.—

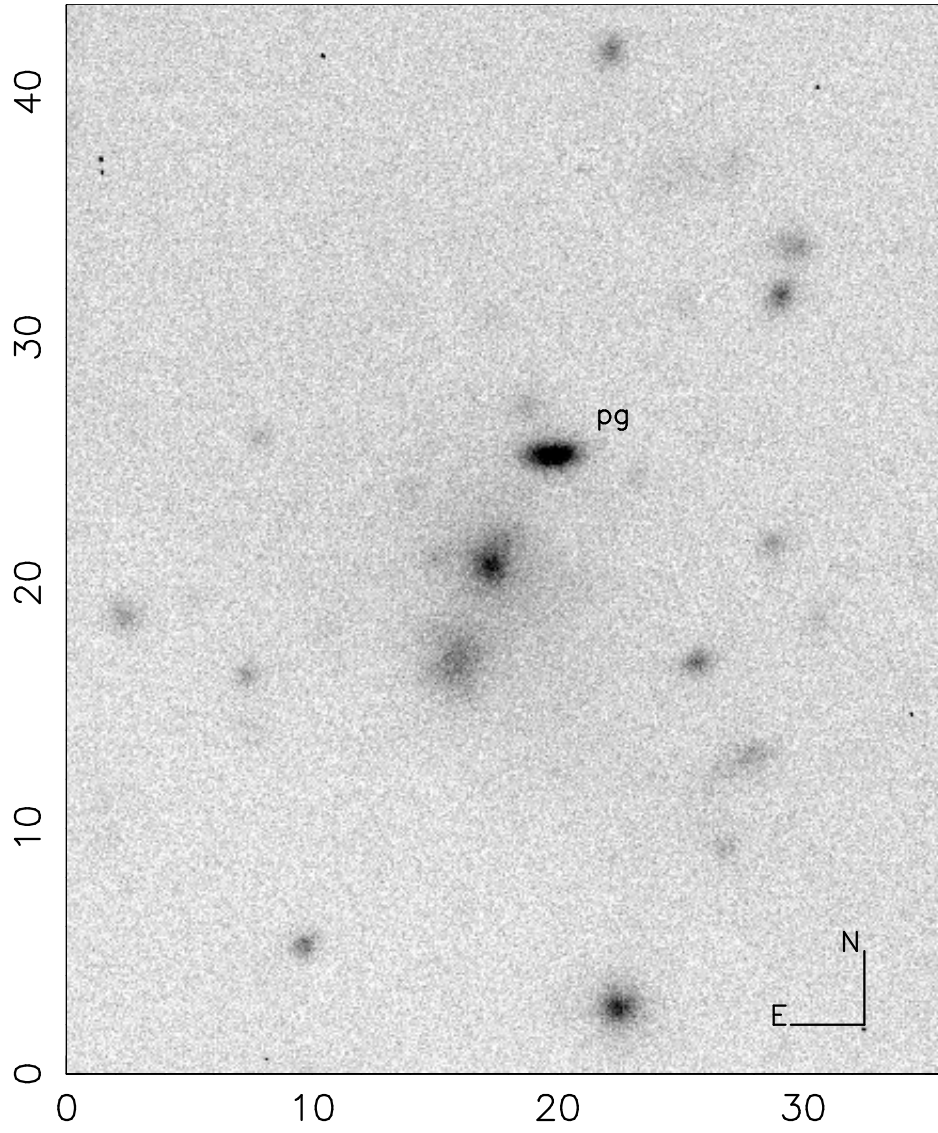


Fig. 2.—

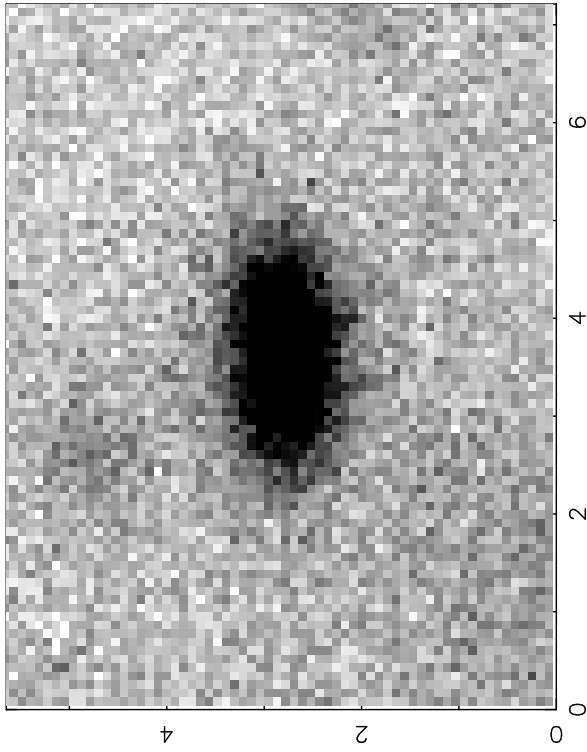
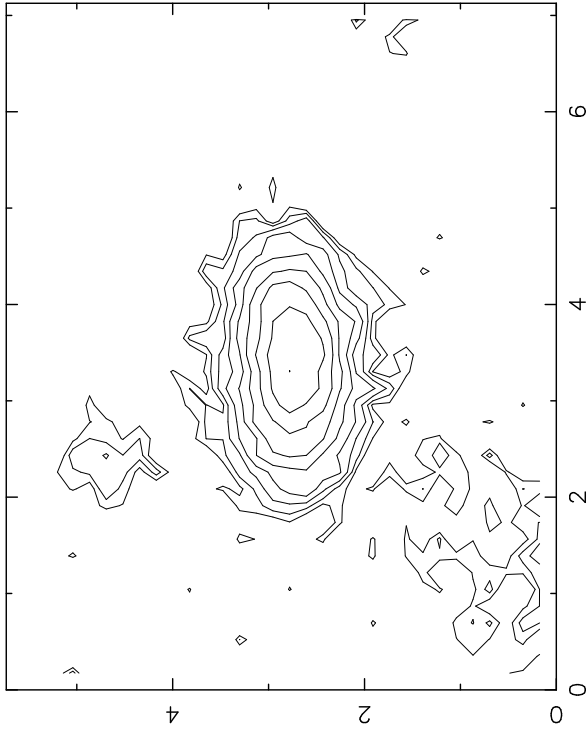


Fig. 3.—

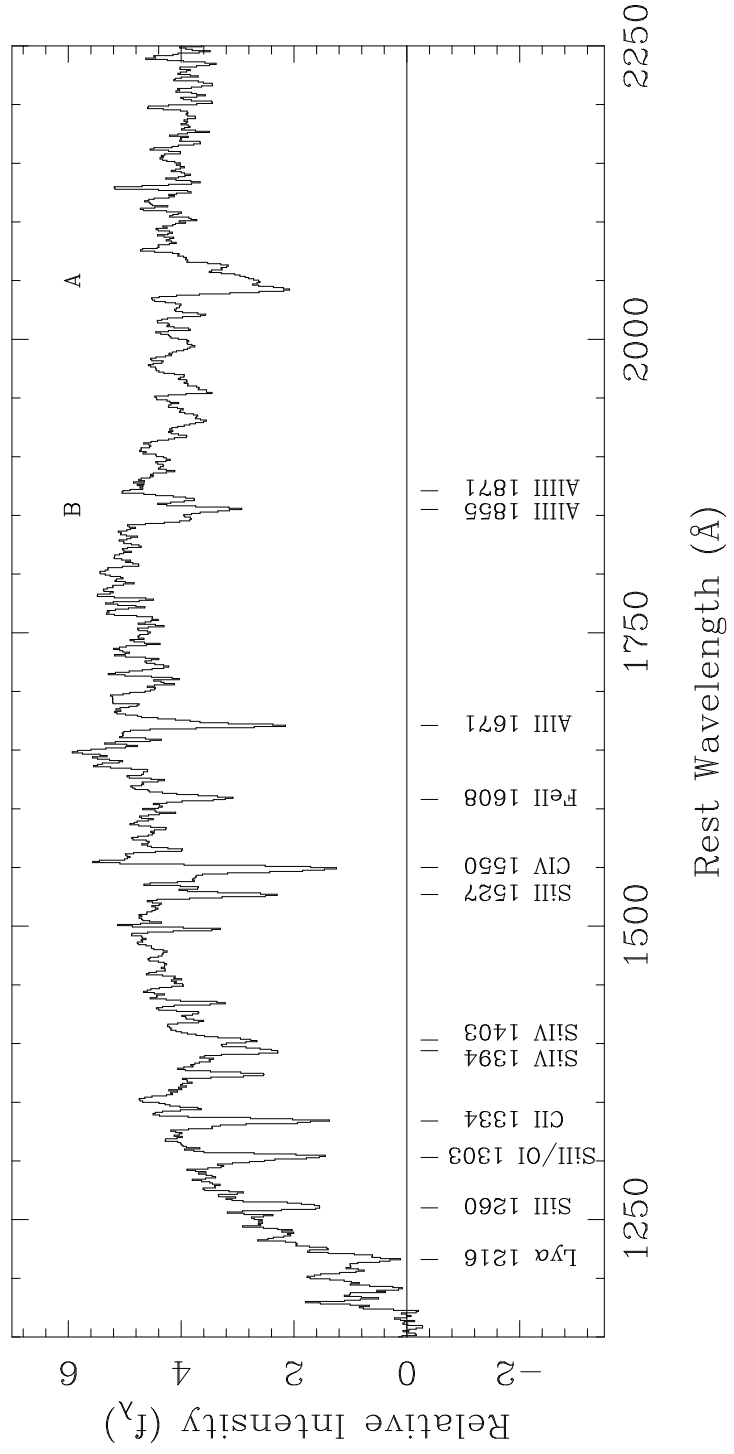


Fig. 4.—

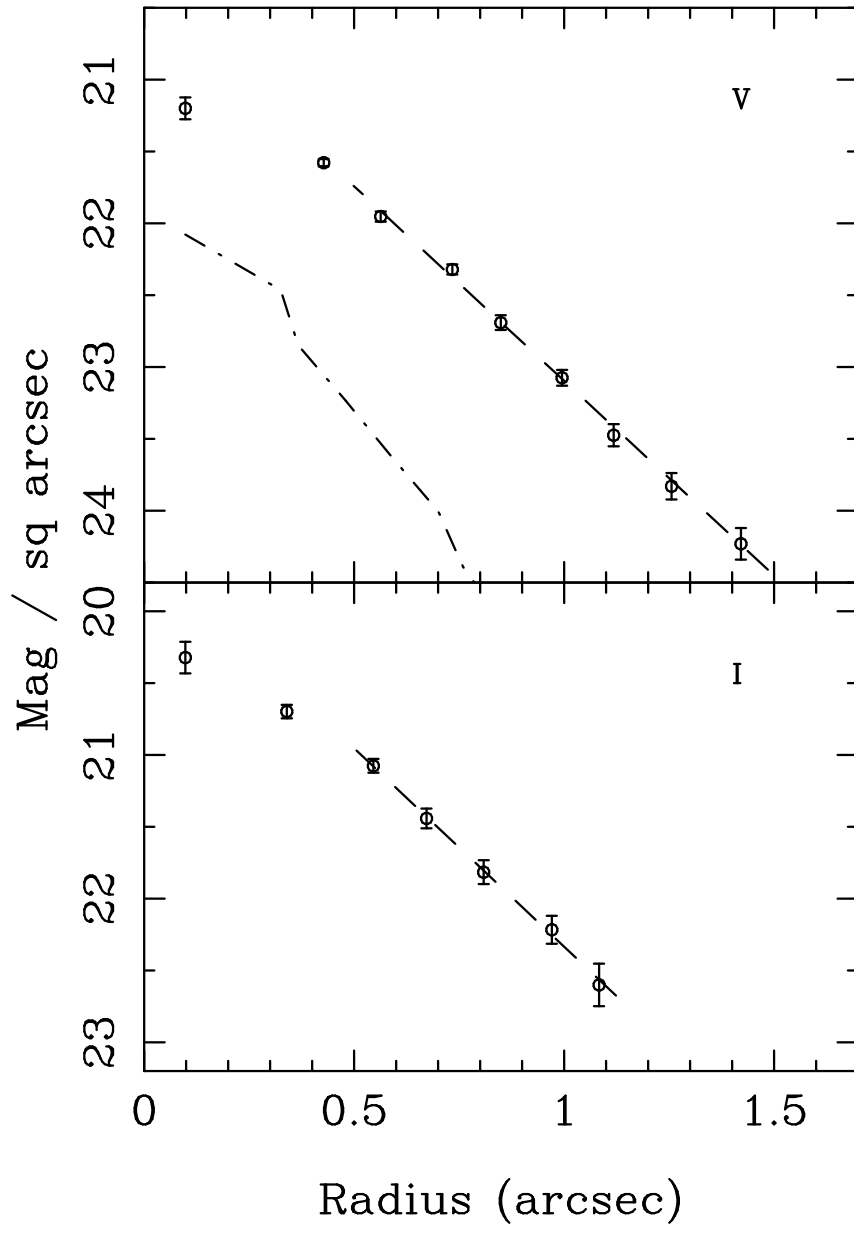


Fig. 5.—

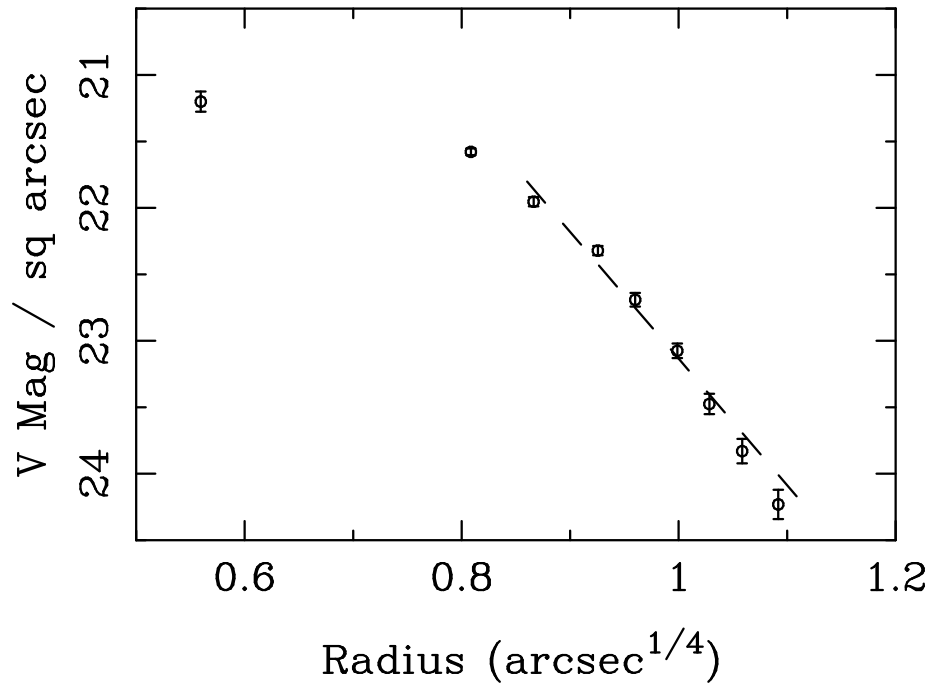


Fig. 6.—

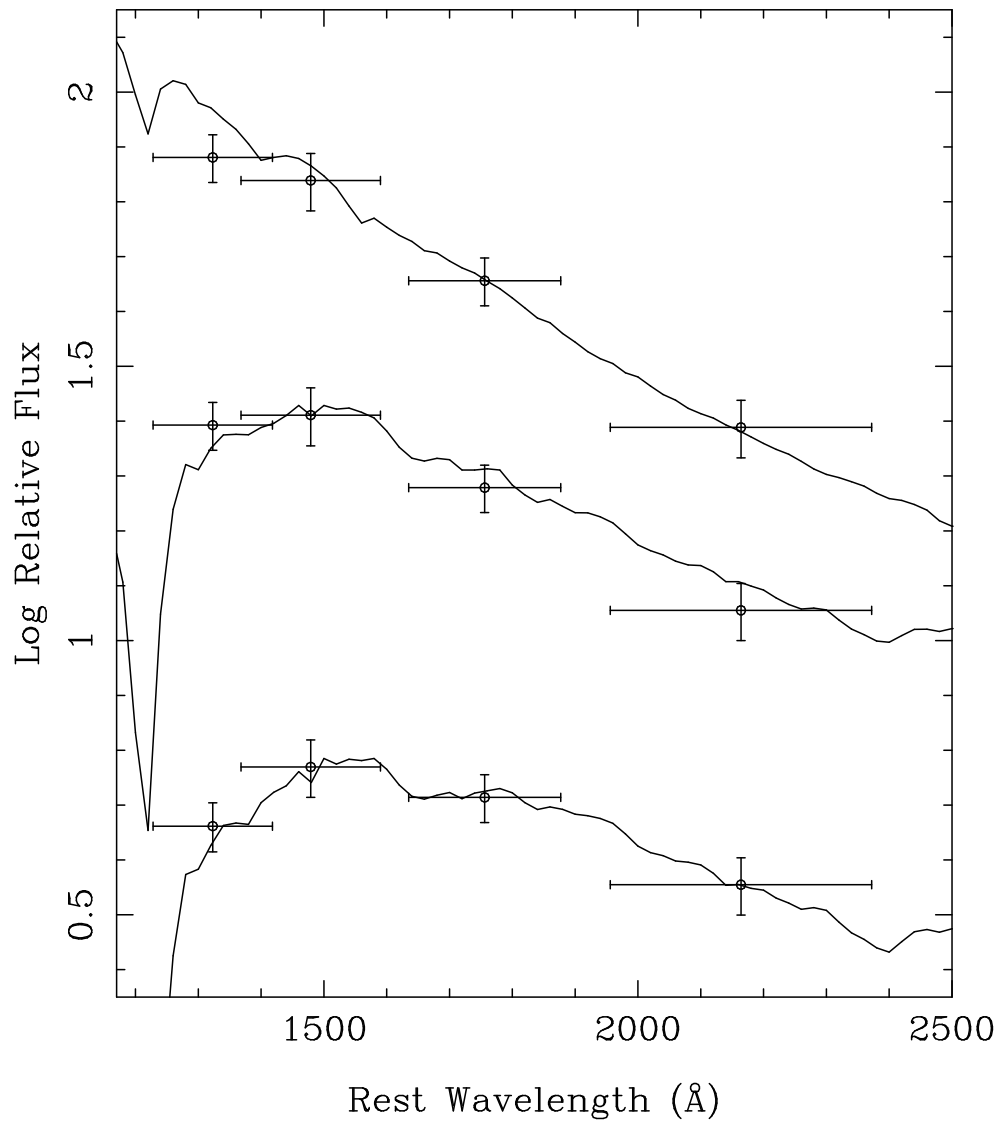


Fig. 7.—

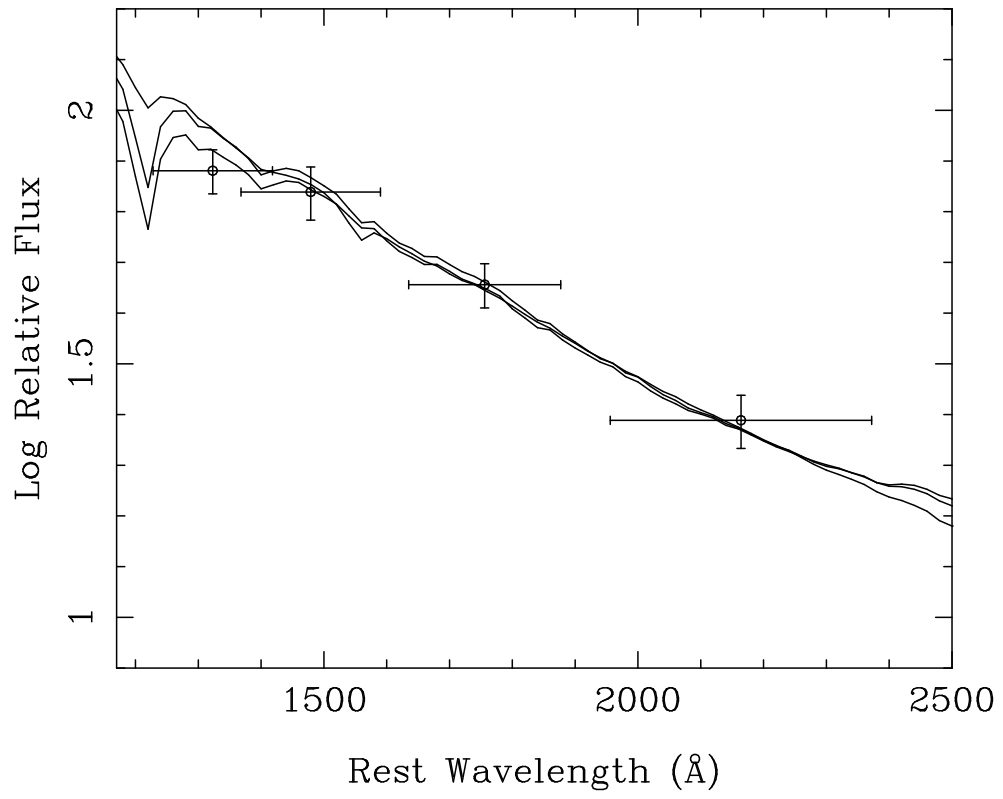


Fig. 8.—

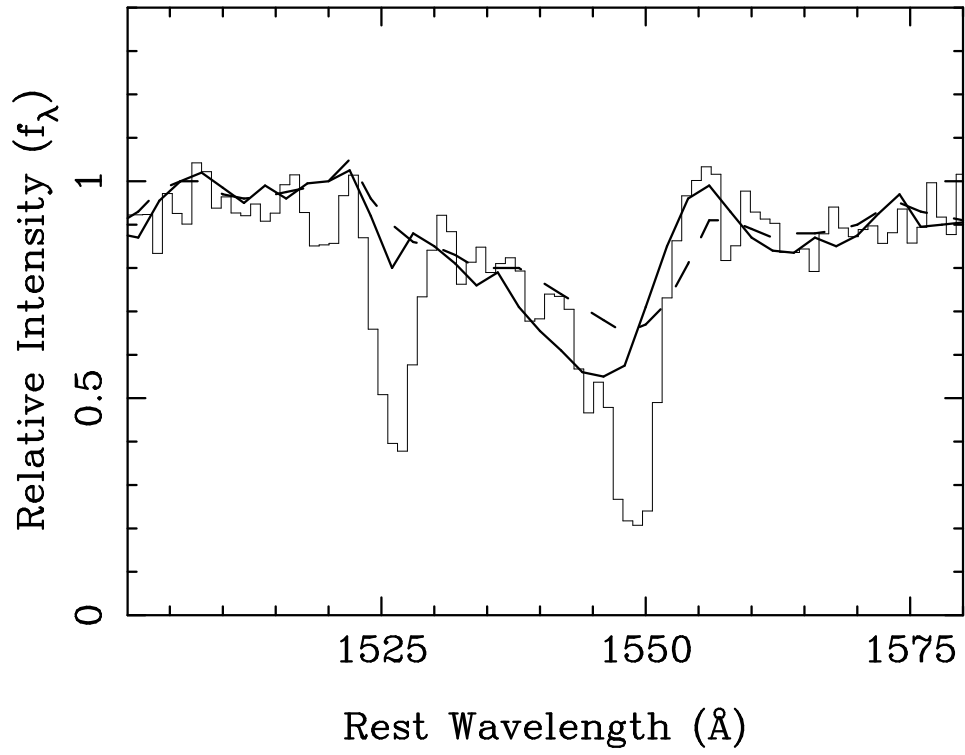


Fig. 9.—